

Ventilation by Displacement in a Three-Dimensional Room— A Numerical Study

LARS DAVIDSON*

Displacement flow systems are becoming popular, especially in Scandinavia, for comfort ventilation. In these systems air is supplied near the floor at low velocity; the temperature of the supply air is a few degrees below that of the air in the room. The supply air is heated by persons and/or machinery in the room. Turbulent plumes are formed above these heat sources. Apart from the plumes, the flow in the room is divided into two zones: a lower zone (the occupied zone) to which clean cool air continuously is supplied, and an upper zone (above the occupied zone) where contaminated warm air is recirculating.

In the present study, the flow in displacement flow systems (a water box model) has been calculated using finite difference methods; the results have been compared with experimental data, and the agreement is reasonably good.

NOMENCLATURE

$C_{1\epsilon}, C_{2\epsilon}, C_\mu$	constants in the turbulence model
G	turbulence generating source term in the k - and ϵ -equations
G_B	turbulence generating source term due to buoyancy in the k - and ϵ -equations
g	acceleration due to gravity
k	turbulent kinetic energy
L	length of a side of the cubical room (see Fig. 2)
n	nominal time constant (= number of air changes per hour)
p	pressure
Q	heat source
S_ϕ	source term of general variable
t	temperature, °C
U, V, W	mean velocity in x -, y - and z -directions, respectively
U_i	mean velocity in x_i -direction
\dot{V}	volumetric flow rate
x	horizontal Cartesian coordinate (see Fig. 2)
x_i	Cartesian coordinate in the i -direction
y	horizontal Cartesian coordinate (see Fig. 2)
z	vertical Cartesian coordinate (see Fig. 2)
z_{front}	the z -level of the front (see Fig. 1)
<i>Greek symbols</i>	
β	coefficient of thermal expansion
τ	time
$\Delta\tau$	time step
Γ_ϕ	exchange coefficient of dependent variable
ϵ	dissipation of turbulent kinetic energy
$\mu, \mu_l, \mu_{\text{eff}}$	dynamic viscosity (laminar, turbulent and effective, respectively)
ρ	density
σ_1	laminar Prandtl number
$\sigma_k, \sigma_t, \sigma_\epsilon$	turbulent Prandtl number for k , t and ϵ , respectively
ϕ	dependent variable

Subscripts

in	inlet
out	outlet
ref	reference value for the room

1. INTRODUCTION

DISPLACEMENT FLOW systems have been used for industries with heavy heat loads for many years [1, 2]. In Scandinavia this type of ventilation system has also become popular for comfort ventilation in rooms; here persons, machinery, lighting etc. constitute the heat loads. The features of this new displacement flow system and the traditional mixing ventilation are given below.

Mixing flow systems. In these systems the air is supplied through a small inlet device near the ceiling (or in the ceiling) at relatively high velocity. A jet, or wall jet, is formed and it entrains the air in the whole room. This gives a nearly uniform distribution of temperature and contaminant throughout the room.

Displacement flow systems. The air is supplied at low velocity through a large inlet device near the floor; the temperature of the supply air is cooler than that in the room. The cool air is heated by the heat source (see Fig. 1). A plume is formed above the heat source due to the higher temperature there (the density is lower) than in its surroundings. The volume flow rate in the plume entrains the surrounding air, and the flow rate in the plume increases with height. At the vertical level z_{front} (the z -level of the front, see Fig. 1) the flow rate in the plume is equal to total ventilation flow rate. The flow in the room is divided into two zones at the front: a lower zone with clean cool supply air, and an upper zone

*Department of Applied Thermodynamics and Fluid Mechanics, Chalmers University of Technology, S-412 96 Gothenburg, Sweden.

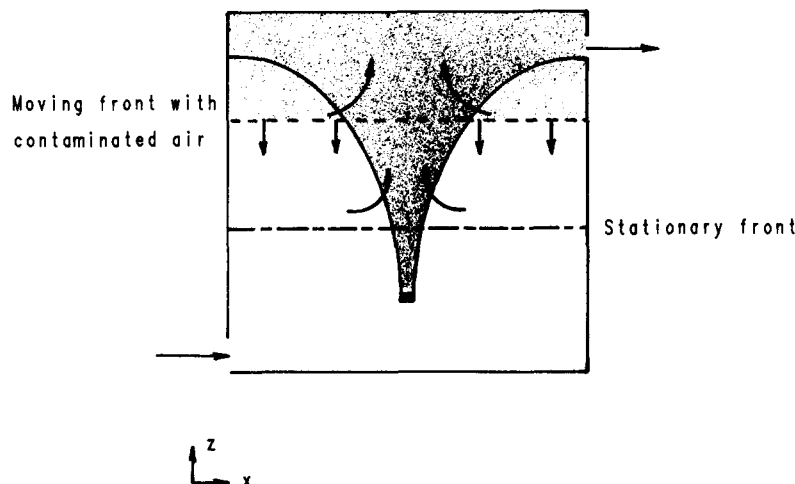


Fig. 1. A schematic figure for a displacement flow system.

where contaminated heated air is recirculating (for further details, see Section 3).

As displacement flow systems are now increasingly replacing the traditional mixing flow systems, it is of great interest to perform a numerical study of the flow in a displacement system. The object of the present study is to calculate the flow in such a configuration using finite-difference methods, and to compare the calculated results with experimental data [3] in order to investigate how well such flows can be predicted using finite-difference methods. No such investigation has, to the best of the author's knowledge, previously been carried out.

The experiments (and the calculations) were carried out in a water box model; water was chosen as medium because it is easier to carry out visualization experiments in water.

The finite difference method used is briefly presented in Section 2, and in Section 3 the function of displacement flow systems is described. Results are given in Section 4, and conclusions are drawn in Section 5.

2. SOLUTION PROCEDURE

The computer program by Davidson and Hedberg [4] has been used. The program solves equations of the type:

$$\frac{\partial}{\partial \tau}(\rho\phi) + \frac{\partial}{\partial x_i} \left(\rho U_i \phi - \Gamma_\phi \frac{\partial \phi}{\partial x_i} \right) = S_\phi, \quad (1)$$

by expressing them in finite difference form. The finite difference equations are solved by a method which is based on the SIMPLEC procedure by Van Doormal and Raithby [5]. The four main features are [6]: (i) use of staggered grids for the velocities; (ii) formulation of the difference equations in implicit, conservative form, using hybrid upwind/central differencing; (iii) rewriting of the continuity equation into an equation for pressure correction, where the latter is used to correct the pressure and the velocities; (iv) iterative solution of the equations.

A transient formulation was adopted as a convenient means of introducing relaxation into the iterative sol-

ution. When only the steady-state solution is of interest, the time step, $\Delta\tau$, is used as a free parameter through which the convergence rate may be optimized.

In the present calculations the dependent variable in equation (1) takes the following forms: U , V , W , t , k , ε and 1 (continuity equation). The corresponding coefficients, Γ_ϕ , and sources, S_ϕ , are defined in Table 1. The Boussinesque approximation was used for the gravitation term in the W -momentum equation.

2.1. Boundary conditions

The xz -plane $y = L/2$ is a symmetry plane (see Fig. 2), and the calculations were consequently carried out in one half of the room only ($0 < y < L/2$). At the symmetry plane zero gradient was imposed for all variables except for the V -velocity, which was set to zero.

Constant profiles were used at the inlet. The inlet velocity and temperature were set according to the experi-

Table 1. Definition of Γ_ϕ and S_ϕ for conservation equations

Equation	ϕ	Γ_ϕ	S_ϕ
Continuity	1	0	0
Momentum	U	μ_{eff}	$-\partial p/\partial x$
Momentum	V	μ_{eff}	$-\partial p/\partial y$
Momentum	W	μ_{eff}	$-\partial p/\partial z + \rho\beta g(t - t_{\text{ref}})$
Temperature	t	$\mu/\sigma_t + \mu_t/\sigma_t$	0
Turbulence energy	k	$\mu_{\text{eff}}/\sigma_k$	$G - \rho\varepsilon + G_B$
Turb. dissipation	ε	$\mu_{\text{eff}}/\sigma_\varepsilon$	$\varepsilon/k[C_{1\varepsilon}(G + G_B) - C_{2\varepsilon}\rho\varepsilon]$

Notes:

$$(1) \quad G \equiv \mu_t \frac{\partial U_i}{\partial x_j} \left(\frac{\partial U_i}{\partial x_j} + \frac{\partial U_j}{\partial x_i} \right);$$

$$\mu_{\text{eff}} = \mu + \mu_t = \mu + C_\mu \rho k^2 / \varepsilon$$

$$G_B \equiv -\frac{g\beta}{\sigma_t} \mu_t \frac{\partial t}{\partial z}$$

(2) Turbulence constants [7]

$$C_\mu = 0.09; \quad C_{1\varepsilon} = 1.44; \quad C_{2\varepsilon} = 1.92;$$

$$\sigma_k = 1.0; \quad \sigma_\varepsilon = 1.3; \quad \sigma_t = 0.9$$

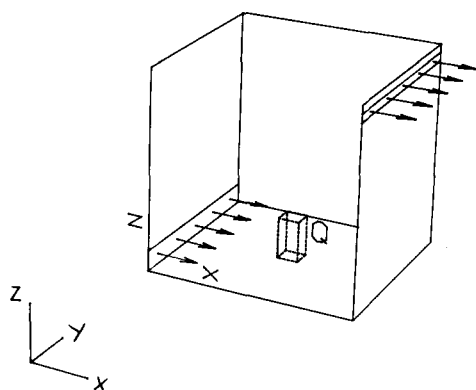


Fig. 2. Configuration. The room is cubical with side-length L ($=0.5$ m). The height of the inlet is $0.2L$. The xz -plane $y = L/2$ is a symmetry plane. A heat source, Q , is introduced (uniformly distributed) in the region bounded by dotted lines in the middle of the room ($0.48 < x/L < 0.52$, $0.48 < y/L < 0.52$, $0 < z/L < 0.22$).

ments; the turbulent quantities were set to zero since the flow through the inlet was considered to be laminar (for $n = 2$ the Reynolds number based on the inlet velocity and height of the inlet was 280).

Conventional wall-functions [7, 8] were used for velocity components parallel to the walls, k and ϵ at all walls; zero heat flux (adiabatic walls) was applied for the temperature.

At the outlet the exit velocity was set according to mass balance and zero stream wise gradient was imposed for the remaining variables.

The heat source in the middle of the room (see Fig. 2) was evenly distributed in the volume bounded by the dotted lines.

2.2. The turbulence model

The standard k - ϵ turbulence model (see Table 1) used in the present study is seen as strictly valid only for fully turbulent flow, which is not the case, for instance, near the inlet of the water box model. There exist low Reynolds number k - ϵ models (for a review, see Patel *et al.* [9]) which are valid in regions where viscous effects are important. The model by Jones and Launder [10], as well as the modified model by Davidson [11], were tested, however these models predict relaminarization (results predicted with the standard k - ϵ model were used as initial fields) throughout the room, which is incorrect.

The models presented in Patel *et al.* [9] have hitherto been used only in flows near walls. These models probably need to be modified in order to be able to handle free recirculating low Reynolds number flow, where the viscous effects are not due to the presence of walls.

3. VENTILATION BY DISPLACEMENT

In displacement flow systems the clean air is supplied through a large inlet near the floor, and the air is extracted near the ceiling; the temperature of the incoming air is a few degrees below that of the room temperature. Figure 1 shows schematically how ventilation by displacement works. The incoming air is heated by persons and/or

machinery in the room, and the heated (and contaminated) air rises due to buoyancy. Above the heat source a turbulent buoyant plume is formed which entrains surrounding air on its way upwards; thus the air flow rate in the plume increases with height. When the air in the plume reaches the ceiling it spreads laterally. As the air flow rate in the plume (\dot{V}_{plume}) is normally much greater than the total ventilation flow rate (\dot{V}_{in}), a fraction ($\dot{V}_{\text{plume}} - \dot{V}_{\text{in}}$) cannot, due to continuity, be extracted through the outlet, but it must turn downwards. At each horizontal plane above the heat source the upward directed air flow rate in the plume must, due to continuity, exceed the downward directed flow rate by the total ventilation flow rate, \dot{V}_{in} . At the z -level where the air flow rate in the plume is equal to the total ventilation flow rate, the downward directed flow will turn upwards again; this z -level is called the *front*.

In this way the flow in the room is divided into two zones.

- (1) The lower zone to which clean air is supplied (except in the plume where contaminated air is moving upwards).
- (2) The upper zone where contaminated air is recirculating.

The plane which divides these two zones is called the *front*. It is, of course, desirable that the front is located above the occupied zone.

As many heat loads are transient (cigarettes, persons entering or leaving the room) it is also of great interest to study the transient behaviour of the ventilation system. During the transient phase the front is moving downwards from the ceiling to its stationary level.

When ventilation by displacement is compared with traditional mixing ventilation, the following points are worth noting.

- (1) In mixing ventilation the contaminants are dispersed evenly in the whole room. This implies that, when the flow is stationary, the conditions in the room are the same as at the outlet. The aim of ventilation by displacement is to keep the contaminants isolated by quickly *displacing* (transporting) them to the region above the occupied zone. In the ideal system this means that the conditions in the occupied zone are the same as in the supplied air.
- (2) Stagnation zones with low ventilation efficiency are often formed in mixing ventilation, whereas in ventilation by displacement this does not usually occur.
- (3) For a given ventilation air flow rate the z -level of the front is strongly dependent on the heat load, and the higher the heat load is, the lower the z -level of the front will be. The location of the front is a crucial parameter for the performance of the displacement flow system. It may happen that the front is located in the occupied zone [12], which, of course, is not desirable.
- (4) In office buildings cooling is needed almost throughout the year (even in Scandinavia!). Since, in

displacement systems, the cool air is in the occupied zone (and the heated air above) less cooling effect (less under-temperature on the supply air) is needed in these systems compared with mixing flow systems.

4. RESULTS

The flow in a three-dimensional room is calculated, see Fig. 2. The width of both the inlet and the outlet is equal to the width of the room. In the middle of the room near the floor a heat source is introduced (dotted region in Fig. 2). The medium is water, and the inlet temperature is around 13°C. Sandberg and Lindström [13] and Sandberg [3] have carried out a number of experimental investigations on this configuration in which vertical temperature profiles have been measured; the calculated results are compared with these data.

The experiments were carried out in a water box model; water was chosen as medium because it is easier to carry out visualization experiments in water. This choice of using a scale model with water as the medium gives different Reynolds and Archimedes numbers compared with a full scale ventilated room with air as the medium. In a full scale room the Reynolds number is two orders of magnitude larger than in the water box model, and the Archimedes number is three orders of magnitude larger. The flow is much more sensitive to the Archimedes number and can, in many cases, be independent of the Reynolds number [14, 15]. The flow pattern in the water box model and a full scale room is the same, as verified by experiments [12, 15]. It thus follows that if the calculated flow pattern agrees with experimental data for the water box model, it will also be the case for full scale rooms.

Heat radiation has been omitted in the present calculations, which is an acceptable approximation since the medium is water and temperature differences are moderate. This may not be the case in a full scale room, where the warm ceiling will give off heat to the walls, and

Table 2. Data for five different cases

Case	Q^*/W	n (h ⁻¹)	U_{in} (m s ⁻¹)	
Q200	200	2	0.00277	steady
Q300	300	2	0.00277	steady
Q400	400	2	0.00277	steady
Q600	600	2	0.00277	transient
n4	600	4	0.00544	steady

*Note that only $Q/2$ is introduced in the calculations, since the calculations are carried out in one half of the room only ($y = L/2$ is a symmetry plane).

especially to the cold floor, which will heat the air near the floor. It is thus probable that the temperature field will be affected by the radiation effect.

Whereas in the water box model the temperature is nearly constant in the lower and the upper zone, the temperature varies linearly with the vertical coordinate in full scale rooms [12, 15]. This is due to radiation and heat flux through the walls in the full scale rooms. As mentioned above, however, experiments showing that the flow pattern is the same in the water box model and in full scale rooms indicate that radiation plays only a minor role for the flow pattern.

The steady flow is calculated for four cases, whereas the transient evolution of the flow is calculated for one case only, see Table 2.

All cases have been calculated using a rather coarse numerical grid with $19 \times 11 \times 18$ nodes. Case Q200 has also been calculated using a finer grid with $35 \times 19 \times 38$ nodes. In all figures presented below, the coarse grid has been used unless otherwise stated.

4.1. Steady calculations

The calculated velocity vectors for Case Q200 are shown in Figs 3–5. It can be seen that the flow goes from

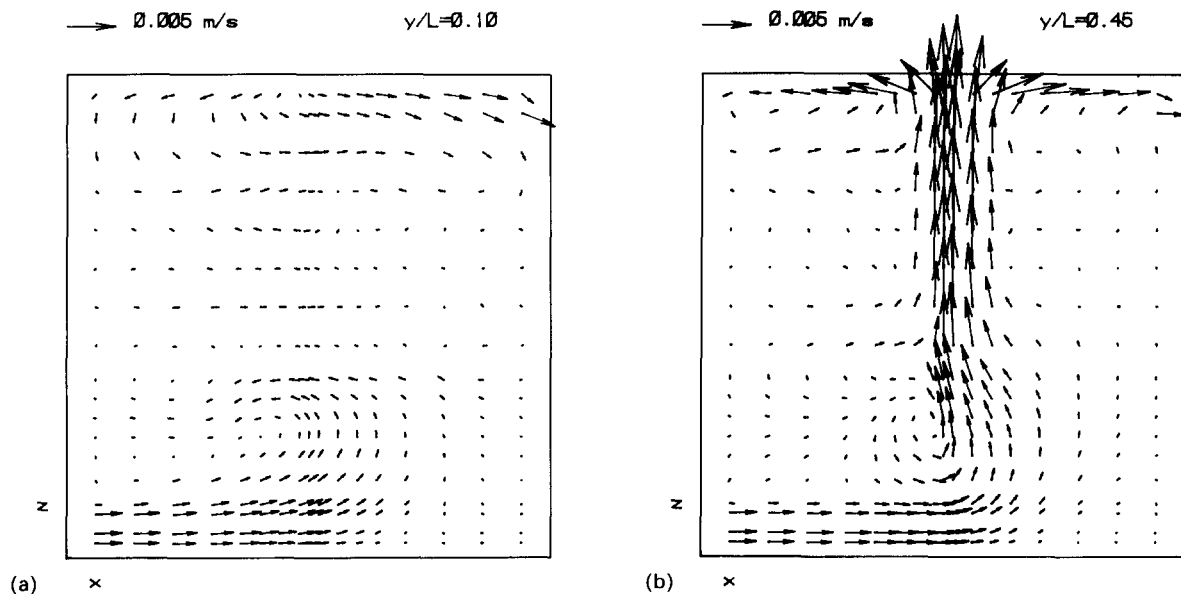


Fig. 3. Calculated velocity vectors; Case Q200; xz -plane. (a) $y/L = 0.1$; (b) $y/L = 0.45$.

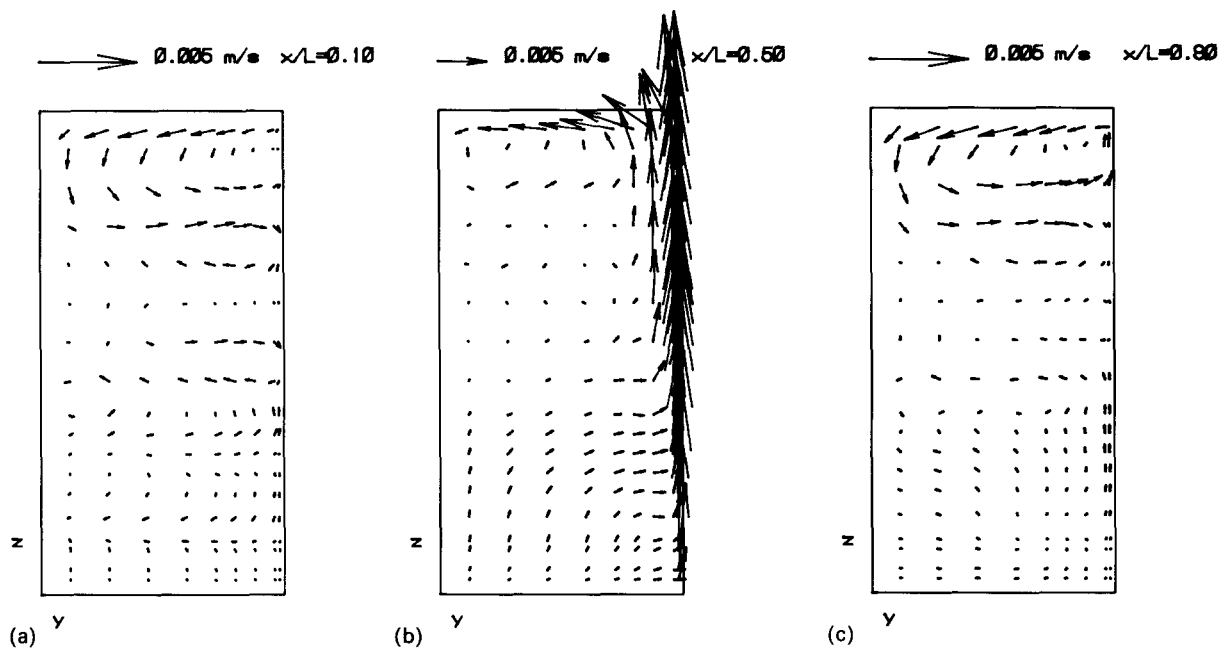


Fig. 4. Calculated velocity vectors; Case Q200; yz -plane. (a) $x/L = 0.1$; (b) $x/L = 0.5$; (c) $x/L = 0.9$.

the inlet towards the opposite wall. Near the heat source ($x/L \approx 0.5$, $y/L \approx 0.5$), the flow is, due to buoyancy, lifted up towards the ceiling, and a turbulent buoyant plume is formed. At the xz -planes where the heat source is introduced ($y/L \approx 0.5$, see Fig. 3b), the direction of the flow is changed from horizontal in the positive x -direction to vertically upwards; in the other xz -planes the direction of the flow is not changed so much, see Fig. 3a.

The calculated velocity vectors shown in Fig. 6 were obtained using the $35 \times 19 \times 38$ -node grid. When these results are compared with those obtained using the $19 \times 11 \times 18$ -node grid (Figs 3-5), it can be seen that the flow patterns are very similar. The calculated temperature profile along a vertical line, obtained with the fine grid, is compared with that obtained with the coarse grid in Fig. 7, and, again, the results predicted using the two grids are very similar.

The calculated temperature profiles along four vertical lines for Case Q200 are compared with experimental data

in Fig. 8a. It can be seen that the calculated results agree well with the experimental data; the experimental temperatures near the ceiling are, however, somewhat higher than the calculated ones. The reason for this may be that in the experiments warm water is trapped at the ceiling because the outlet is situated at some distance below the ceiling, or it may be that the ceiling is insufficiently insulated (the surrounding room temperature in the experiments was approximately 20°C [3]).

In Fig. 8b the calculated temperature profiles for Case Q600 are compared with experiments. Here the experimental values are larger than the calculated ones. It should be noted that this already is the case near the floor, which might be due to the possibility that in the experiments the water has been heated on its way from the inlet to the measuring points (which are located near the wall opposite the inlet). This heat may come from outside the water box model due to insufficient insulation of the walls, or it may be that heat diffuses from the plume or from the upper part of the room to this region.

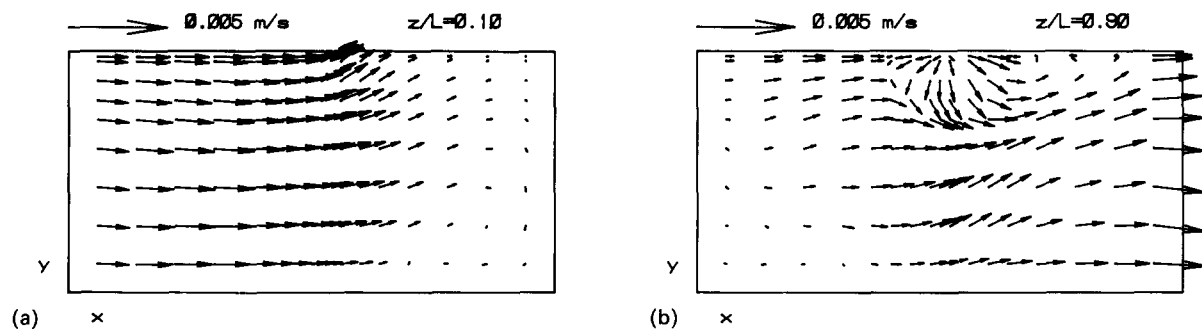


Fig. 5. Calculated velocity vectors; Case Q200; xy -plane. (a) $z/L = 0.1$; (b) $z/L = 0.9$.

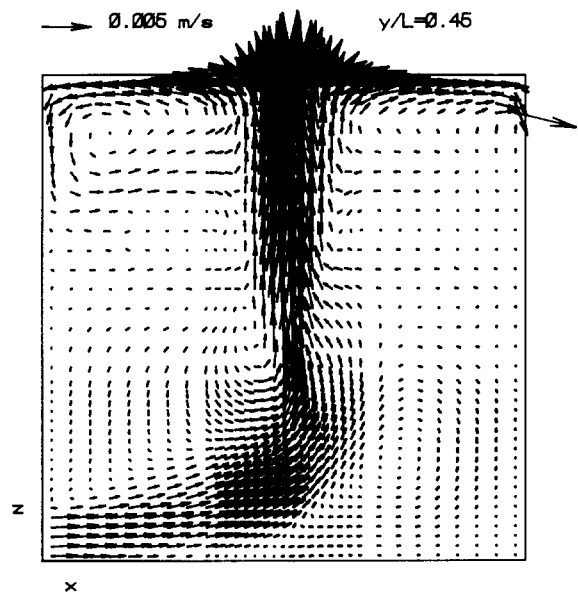


Fig. 6. Calculated velocity vectors; Case Q200; fine grid; xz -plane; $y/L = 0.45$.

The question of how well the walls are insulated in the experiments is easily answered by checking how well the global heat balance is satisfied [heat source = $\rho \dot{V}_{in} (t_{out} - t_{in})$]. In Case Q200, 68 W is leaking through the walls, and in Case Q600 90 W. In the former case most of the heat seems to come through the ceiling. The diffusion from the plume and/or from the upper part of the room is probably more important in Case Q600 than in Case Q200, since the turbulent diffusion is larger in Case Q600, due to the velocities and the velocity gradients being larger. Another problem in the experiments for Case Q600 is that the inlet temperature drifts between 12.5 and 12.8°C; $t_{in} = 12.6$ has been used in Fig. 8b (as well as in Figs 14 and 15, see below). This drift of the inlet temperature can also be the reason why the experimental

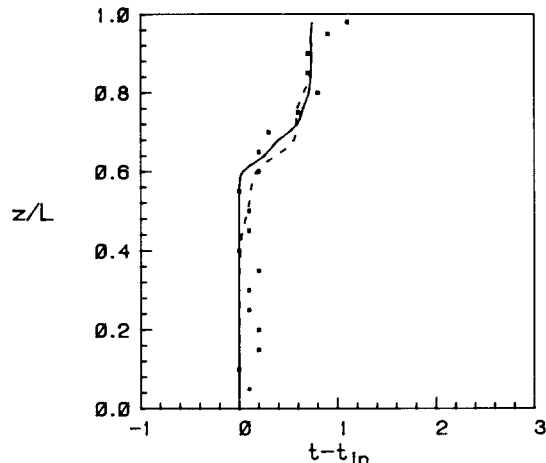


Fig. 7. Temperature profiles along a vertical line at $x/L = 0.5$, $y/L = 0.1$. Case Q200. Solid line: calculations, fine grid; dashed line: calculations, coarse grid; markers: experiments [3].

temperatures near the floor are higher than the calculated ones. Despite the discrepancies between the experimental and the calculated temperature profiles, their *form* is very similar.

It is further seen in Fig. 8 that the calculated temperature profiles are all very similar, which shows that the temperature is nearly a function of z only, i.e. $t = \text{function}(z)$.

Horizontal W -velocities and temperature profiles for the planes $x/L = 0.5$ and $y/L = 0.5$ are presented in Figs 9 and 10. Outside the plume, it is striking how constant both the W -velocity (which is close to zero) and the temperature are. The flow is very stratified outside the plume, and moves horizontally along the isothermals; this was also found by the author [16], where the flow in three-dimensional thermally ventilated rooms was calculated. Further it can be seen (in Figs 9 and 10) that the profiles predicted with the two different grids differ rather much from each other. The profiles predicted with the

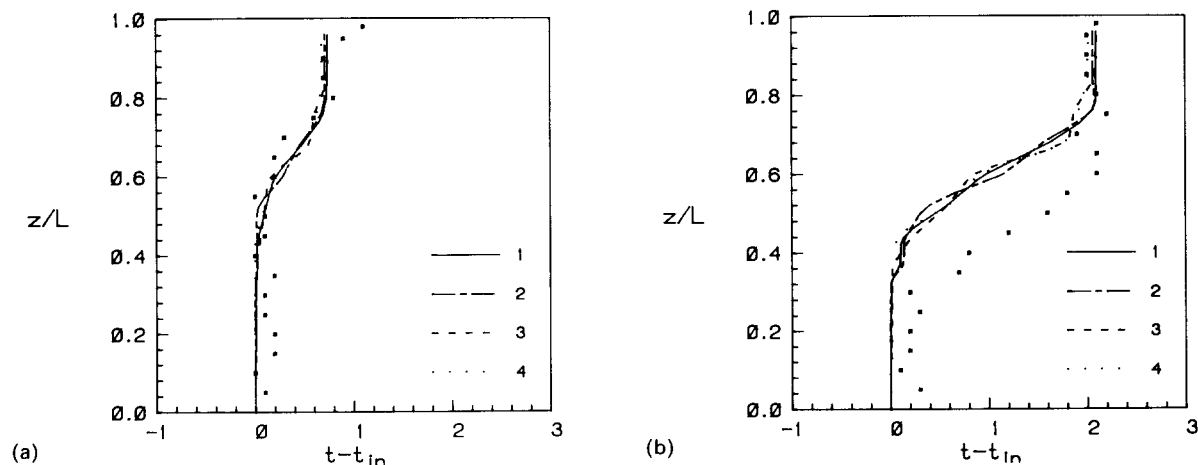


Fig. 8. Temperature profiles along vertical lines. Line (1) $x/L = 0.1$, $y/L = 0.1$; line (2) $x/L = 0.9$, $y/L = 0.1$; line (3) $x/L = 0.1$, $y/L = 0.4$; line (4) $x/L = 0.9$, $y/L = 0.4$. Markers: experiments [3]. (a) Case Q200; (b) Case Q600 (steady state).

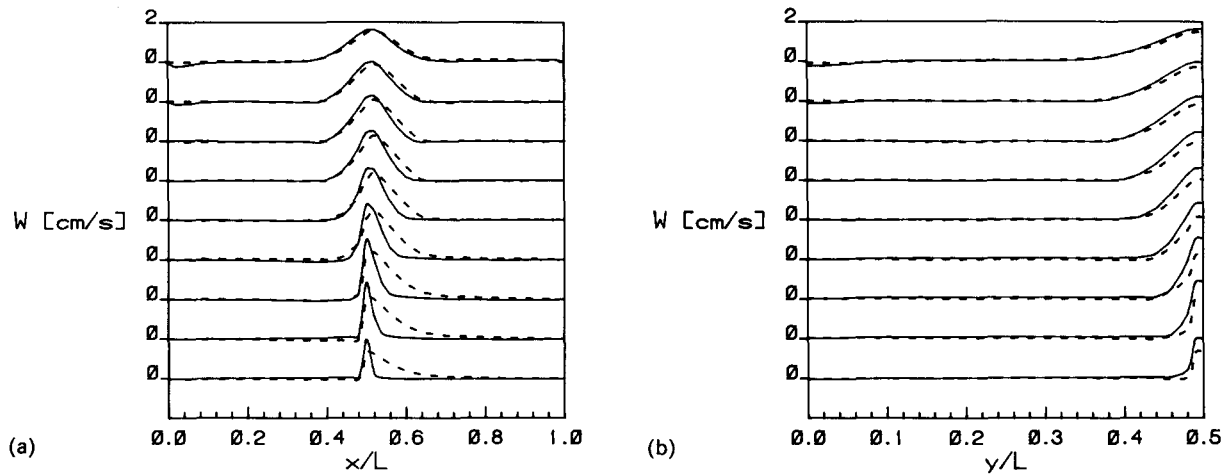


Fig. 9. Calculated horizontal W -velocity profiles. $z/L = 0.1, 0.2, \dots, 0.9$. Case Q200. Solid lines: fine grid; dashed lines: coarse grid. (a) xz -plane, $y/L = 0.5$; (b) yz -plane, $x/L = 0.5$.

coarse grid are somewhat asymmetrical around the mid-plane $x/L = 0.5$, which shows that the plume is affected by the inlet wall jet, and that the plume is pushed away from the inlet by the wall jet. This phenomenon is, however, caused by the coarseness of the grid. Despite these differences between the predictions with the two grids, the predicted values of the z_{front} differ not more than 5% (see below).

A parameter which is of great interest to an engineer who is designing a displacement flow system is the flow rate in the plume; when this parameter is known the value of the z_{front} is easily obtained ($z = z_{front}$ where $\dot{V}_{plume} = \dot{V}_{in}$). The flow rate in the plume as a function of the vertical coordinate, z , is shown in Fig. 11, and, as can be seen, the discrepancy between the flow rate predicted with the two grids is rather large; this was to be expected, as the W -velocities in Figs 9a and b are rather different. The flow rate in the plume as a function of z was cal-

culated as:

$$\dot{V}_{plume}(z) = \int_{\delta A(z)} W(x, y, z) dA, \quad W(x, y, z) > \lambda W_{max}(z).$$

The area of the plume, $\delta A(z)$, in the integral is thus defined as the region where the W -velocity at the z -level in question is larger than $\lambda W_{max}(z)$ [$W_{max}(z)$ is the maximum W -velocity at level z]. The factor λ was chosen as 0.05; an increase of λ to 0.1 altered the calculated flow rate less than 5%. According to Chen and Rodi [17] the flow rate in a plume varies as z^m where $m = -5/3$; the flow rate predicted with the fine grid gives $m = -1.52$ for $z/L < 0.6$. For larger z the flow rate increases at a much lower rate, because the temperature difference between the plume and its surroundings (which is the driving potential for the plume) decreases.

From the flow rate in the plume the value of the z_{front}

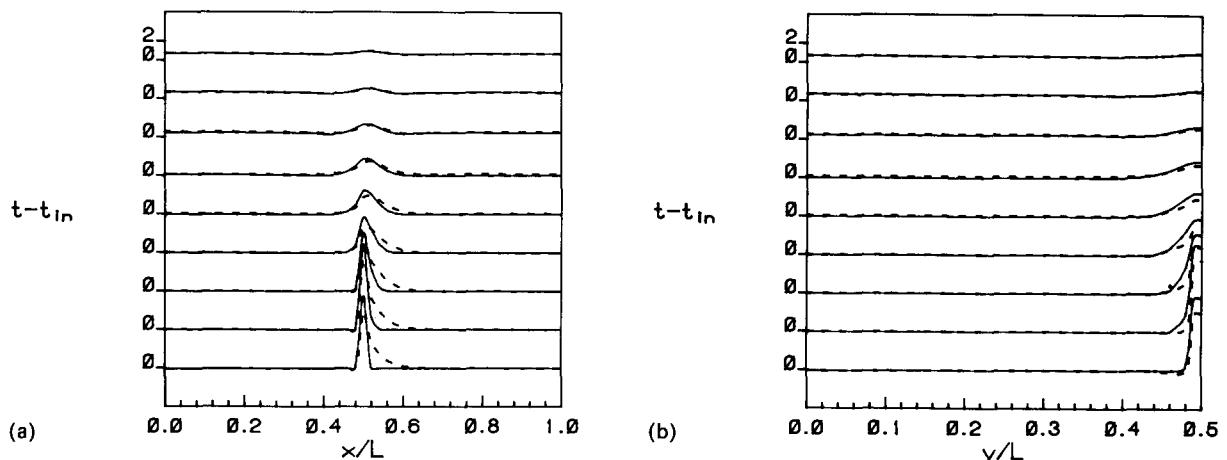


Fig. 10. Calculated horizontal temperature profiles. $z/L = 0.1, 0.2, \dots, 0.9$. Case Q200. Solid lines: fine grid; dashed lines: coarse grid. (a) xz -plane, $y/L = 0.5$; (b) yz -plane, $x/L = 0.5$.

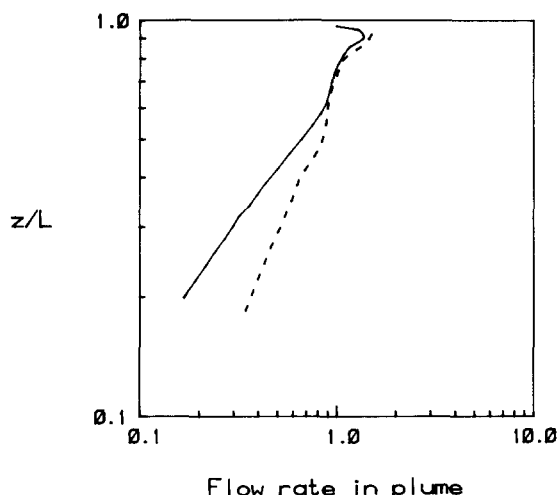


Fig. 11. Calculated flow rate in the plume scaled with the total ventilation flow rate. Case Q200. Solid line: fine grid; dashed line: coarse grid.

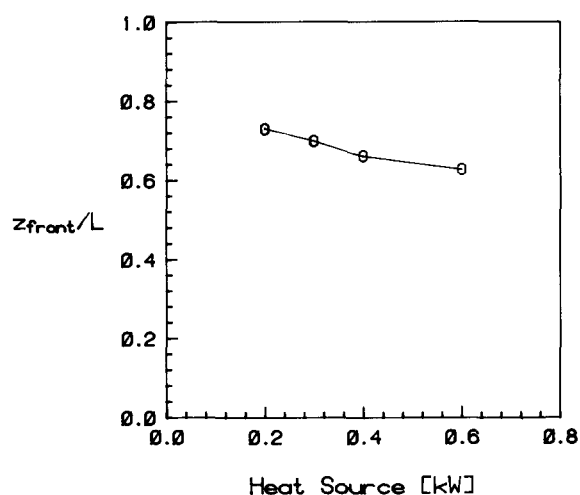


Fig. 12. Calculated z_{front}/L as a function of the heat load. Cases Q200, Q300, Q400, Q600 (steady state).

is, as mentioned above, easily calculated. For the coarse grid $z_{front}/L = 0.74$ is obtained, and for the fine grid, $z_{front}/L = 0.68$ (Case Q200); for Case Q600 the value 0.62 is obtained.

It is not clear how to define the experimental value of the z_{front} from temperature profiles; if the z_{front} is defined as the average of the two levels where:

(i) the temperature exceeds the inlet temperature by Δt ; and

(ii) the temperature is Δt below the temperature at the ceiling or, rather, below the outlet;

where Δt is, say, 0.1°C , then the experimental values $z_{front}/L \approx 0.45$ for Case Q600, and $z_{front}/L \approx 0.7$ for Case Q200 are obtained. The calculated value thus agrees well for Case Q200, but less well for Case Q600. It is hard to tell whether this discrepancy is due to inaccuracies in the experiments or in the calculations, and it should be remembered that the front is not very distinct for this case, since the temperature increase from minimum to maximum occurs over a very long distance ($\approx 0.4L$).

What happens when the heat load is increased? The velocity and the flow rate in the plume should increase and, consequently, the value of the z_{front} should decrease. This is because the larger the heat source, the larger the flow rate in the plume, and the lower the z -level where the flow rate in the plume is equal to the total ventilation flow rate, i.e. where $z = z_{front}$ (see Section 3). In Fig. 12 the calculations with different heat loads (Q200, Q300, Q400, Q600) are presented. It is seen that the value of the z_{front} does decrease with increasing heat load as expected.

Whereas a higher heat load gives a lower value of the z_{front} , a larger total ventilation flow rate (higher inlet velocity) gives the opposite result: a higher position of the front. Calculations with different inlet velocities were carried out in order to plot the position of the front versus the number of air changes/hour, n . It was found, however, that the inlet wall jet disturbs the plume for high velocities, see Fig. 13. It can be seen that near the floor the wall jet passes the heat source (at $x/L = 0.5$) without being lifted (compare Figs 3b and 6).

4.2. Transient calculation

As the heat loads in ventilated rooms very often change (people entering and leaving the room, computer terminals being turned on/off), it is also of great interest to study the transient behaviour of a displacement flow system. An interesting parameter is, of course, the z_{front} : how does the z_{front} vary with time, and does the zone above the z_{front} reach down into the occupied zone during time periods of heat load?

Case Q600 has been calculated transiently, and the temperature profiles are presented in Figs 14 and 15. In Fig. 14 the calculated temperature profiles for $\tau = 15, 30$,

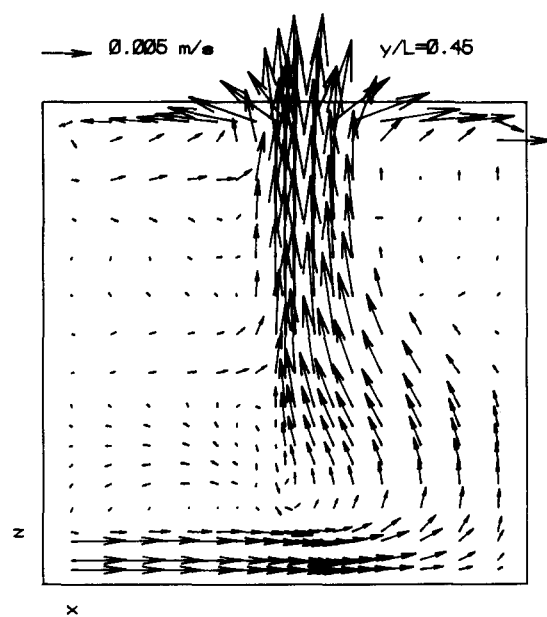


Fig. 13. Calculated velocity vectors. Case n4. xz -plane, $y/L = 0.45$.

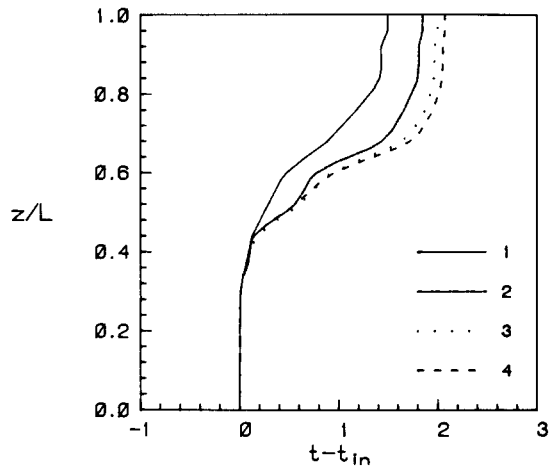


Fig. 14. Calculated vertical temperature profiles. Case Q600. Line (1) $\tau = 15$; line (2) 30; line (3) 45; line (4) 60 min.

45 and 60 min are plotted. The temperature increases with time as was expected. It can be seen from Fig. 14 that the zone above the z_{front} does extend with time. In Fig. 15 the calculated temperature profiles are compared with experimental data; even if the temperature profiles

differ rather much, it is seen that the zone above the z_{front} extends downwards with time in both experiments and calculations.

4.3. Computational details

All calculations have been performed on a VAX 2000, which is about half as fast as a VAX 785 for this type of application. The CPU time required for a convergent solution varied between 26 h (Case Q200) and 48 h (Case Q600, transient) using the coarse grid. The CPU time using the fine grid was approximately 80 h. Time steps of five seconds were used, and two to four thousand time steps were needed in order to get a convergent solution.

It is well known that for buoyancy driven flows (as in displacement flow systems) it is hard to get convergent solutions [18, 19]. For Case Q600 no steady solution could be obtained, but the flow had to be calculated transiently. The time variation of the flow was, of course, very small after 60 min in real time (see Fig. 14).

5. CONCLUSIONS

The flows in displacement flow systems have been calculated and compared with experimental data. The predicted flow pattern was shown to agree reasonably well with experiments. The calculated results show the typical,

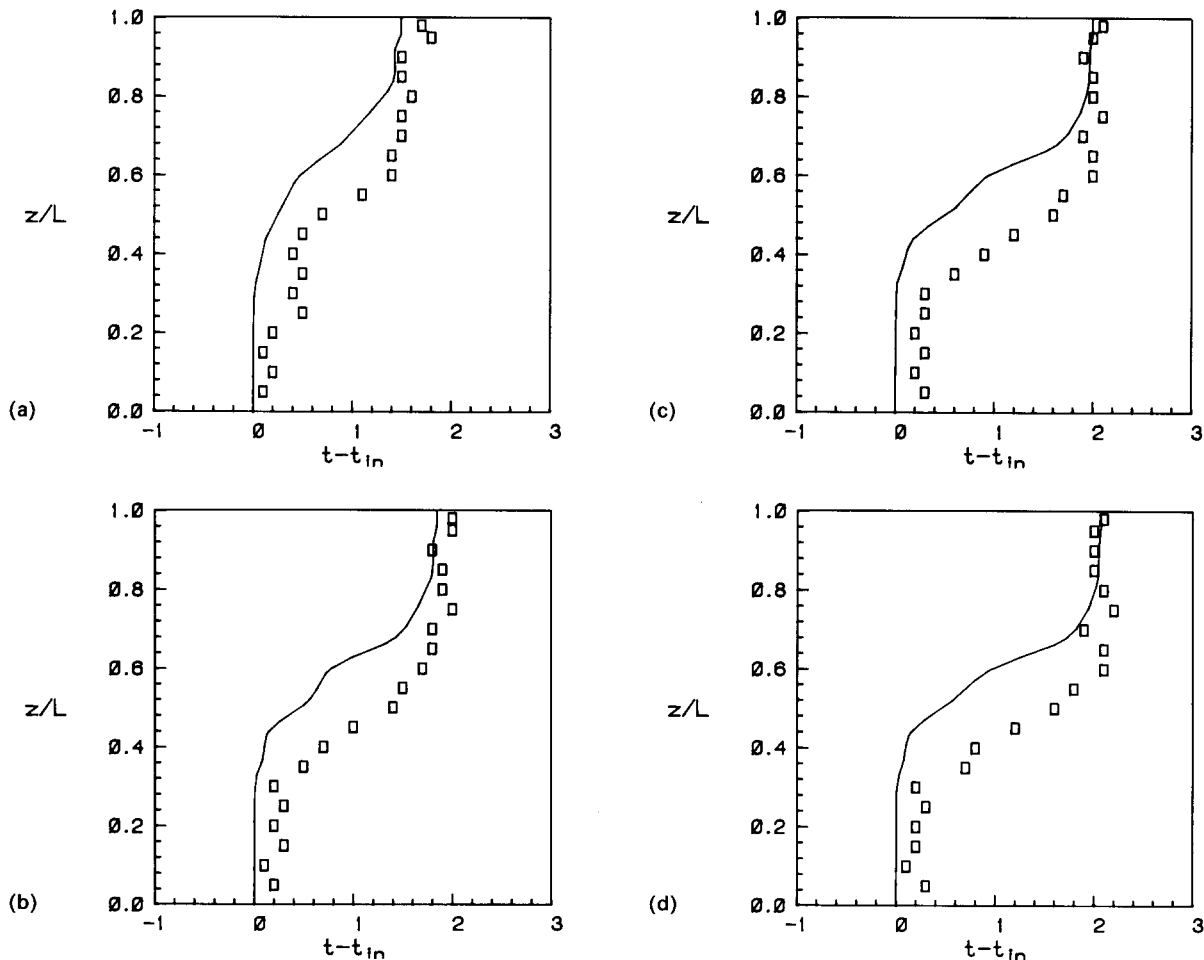


Fig. 15. Calculated vertical temperature profiles compared with experiments [3]. Case Q600. Lines: calculations; markers: experiment. (a) $\tau = 15$; (b) 30; (c) 45; (d) 60 min.

for displacement flow systems, division of the flow into two zones: one lower well ventilated zone, and one upper zone where warm fluid is recirculating. The calculated temperature profiles have been compared with experimental ones, and the agreement was good in one case (Case Q200), but less good in Case Q600. It is hard to tell whether the reason for this discrepancy is inaccuracies in the experiments or in the calculations.

The z-level of the front (see Fig. 1) was well predicted in Case Q200 (it differed less than 5% from the experimental value), but it was less well predicted in Case Q600 (25% lower than the experimental value). The front is, however, not very distinct for this latter case, since the temperature increase from minimum to maximum occurs over a very long distance ($\approx 0.4L$).

The present calculations have been carried out in a water box model [3], which has different Reynolds numbers and Archimedes numbers than a full scale room with air as medium. There is a need for more numerical studies of the flow in full scale rooms in order to further investigate the feasibility of finite-difference methods in calculating the flow in displacement flow systems; in such calculations, heat radiation effects should be taken into account.

Acknowledgements—The author wishes to thank Dr. Mats Sandberg at the National Swedish Institute for Building Research, who has been very helpful. The author is also grateful to Professor Erik Olsson for his help and support. The Swedish Council for Building Research has sponsored this work.

REFERENCES

1. R. A. Beier and R. L. Gorton, Thermal stratification in factories—cooling loads and temperature profiles. *ASHRAE Trans.* **84**, 325–338 (1978).
2. T. E. Kreichelt, G. R. Kern and F. B. Higgins Jr, Natural ventilation in hot process buildings in the steel industry. *Iron Steel Engr.* 39–46 (1976).
3. M. Sandberg, Private communication. National Swedish Institute for Building Research, Gävle, Sweden (1988).
4. L. Davidson and P. Hedberg, A general computer program for transient, three-dimensional, turbulent, recirculating flows. Rept. 86/13, Dept of Applied Thermodynamics and Fluid Mechanics, Chalmers University of Technology, Göteborg (1986).
5. J. P. Van Doormaal and G. D. Raithby, Enhancements of the SIMPLE method for predicting incompressible fluid flows. *Numer. Heat Transfer* **7**, 147–163 (1984).
6. S. V. Patankar, *Numerical Heat Transfer and Fluid Flow*. McGraw-Hill, New York (1980).
7. W. Rodi, *Turbulence Models and Their Application in Hydraulics*. International Association of Hydraulic Research, Monograph, Delft, The Netherlands (1980).
8. L. Davidson, Numerical simulation of turbulent flow in ventilated rooms. PhD thesis, Dept of Applied Thermodynamics and Fluid Mechanics, Chalmers University of Technology, Göteborg (1989).
9. V. C. Patel, W. Rodi and G. Scheuerer, Turbulence models for near-wall and low Reynolds number flows: a review. *AIAA J.* **23**, 1308–1319 (1986).
10. W. P. Jones and B. E. Launder, The prediction of laminarization with a two-equation model of turbulence. *Int. J. Heat Mass Transfer* **15**, 301–314 (1972).
11. L. Davidson, Calculation of the turbulent buoyancy-driven flow in a rectangular cavity using an efficient solver and two different low Reynolds number $k-\epsilon$ models. Rept, Dept of Applied Thermodynamics and Fluid Mechanics, Chalmers University of Technology, Göteborg (1989).
12. M. Sandberg and C. Blomqvist, Displacement ventilation systems in office rooms. *ASHRAE Trans.* (1989).
13. M. Sandberg and S. Lindström, A model for ventilation by displacement. Proceedings: Room Ventilation '87—International Conference on Air Distribution in Ventilated spaces, Stockholm, Sweden (1987).
14. P. V. Nielsen, Flow in air-conditioned rooms (English translation of PhD thesis, Technical University of Denmark, 1974), Danfoss A/S (1976).
15. P. V. Nielsen, Displacement ventilation in a room with low-level diffusers. Kälte-Klima-Tagung, Deutscher Kälte- und Klimatechnischer Verein, Munich (1988).
16. L. Davidson and E. Olsson, Calculation of age and local purging flow rate in rooms. *Bldg Envir.* **22**, 111–127 (1987).
17. C. J. Chen and W. Rodi, *Turbulent Buoyant jets—A Review of Experimental Data*. Pergamon Press, Oxford (1979).
18. I. P. Jones, The convergence of a simple iterative strategy for strongly stratified flows. Proceedings of the 4th International Conference on Numerical Methods in Laminar and Turbulent Flow, Swansea, Vol. 1, pp. 733–740 (1985).
19. P. F. Galpin and G. D. Raithby, Numerical solution of problems in incompressible fluid flow: treatment of the temperature–velocity coupling. *Numer. Heat Transfer* **10**, 105–130 (1986).